DYNAMIC BEHAVIOR OF COMPOSITE SHIP STRUCTURES (DYCOSS)

FAILURE PREDICTION TOOL

Paul Lemmen[1], Gert-Jan Meijer[1], Erik A. Rasmussen[2]

[1] TNO Center for Mechanical Engineering
P.O.Box 49, NL-2600 AA Delft, the Netherlands
+31 15 269 5376; P.Lemmen@bouw.tno.nl

[2] Naval Surface Warfare Center, Carderock Division
9500 MacArthur Boulevard, West Bethesda MD 20817-5700
(301) 227 1656; RasmussenEA@nswccd.navy.mil

This paper is concerned with methods for modeling progressive failure in dynamically loaded ship hull structures of laminated composite materials. Attention is focussed to joints, as these are most susceptible to failure. Three failure modes are considered: delaminations along secondary bondlines, cracking of inserts made of isotropic materials and delamination of the composite material itself. Because of principal differences in their nature, separate models have been defined for each of these modes. The methods are implemented in the DYNA3D explicit finite element code. Their performance is illustrated by two applications.

INTRODUCTION

Over the past few decades fibre reinforced plastics (FRP) have found more and more applications in naval structures. Examples involve decks, superstructures, landing crafts and mine countermeasure vessels. In many of these applications questions arise about the reliability of a design during a shock or blast event. Analyzing the failure behavior, however, is complicated. Not only are there a large number of variables involved, often a qualitative link between the structural behavior and numerical models is missing. The failure mechanisms and modes are often unknown and so are the related parameters.

The failure of composite ship structures exposed to underwater explosions is being investigated in the joint NL-US program DYCOSS (Dynamic Behavior of Composite Ship Structures). In this program a systematic approach for the validation of structural designs has been developed [1]. For a given structural concept, the procedure begins by first identifying predominant failure modes through the use of sunken box underwater explosion tests. The sunken box tests and additional shock table tests are then simulated using a computational tool that can describe the observed damage patterns. Sensitivity studies are performed to obtain a set of material parameters that provides good correlation between experimental and numerical data. The obtained parameters may then be used to analyze the design under investigation. The numerical studies are performed using detailed models assuming plane strain conditions. Test arrangements have been designed to provide 2-D deformation patterns. See Figure 1.

The computational tool mentioned above has been developed under DYCOSS. It consists of a set of methods, specifically an element formulation in combination with an adequate constitutive model, implemented in the finite element program DYNA3D [2]. The set of methods is referred to as the Failure Prediction Tool (FPT). Three failure modes have been considered: debonding; cracking of fillets and inserts; and delamination of the composites themselves. Each method employs a softening relationship between stresses and strains in describing the brittle

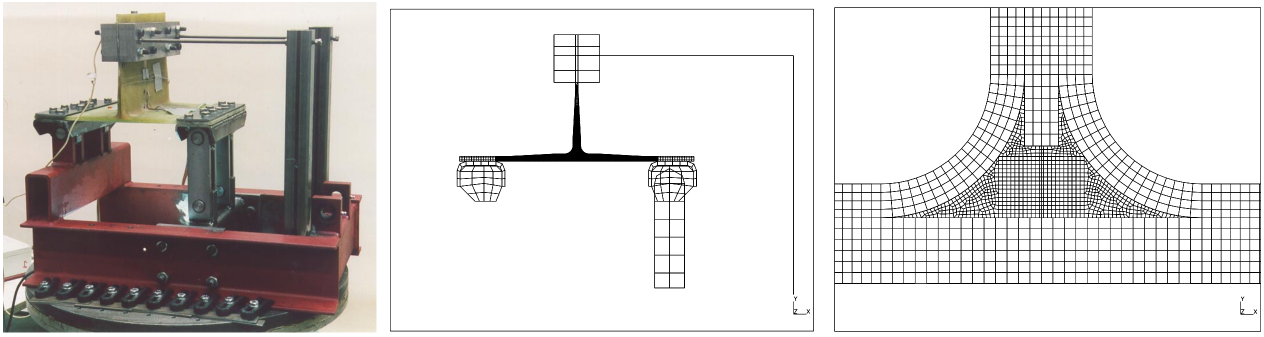

Figure 1 Test arrangement on shock table and corresponding finite element model

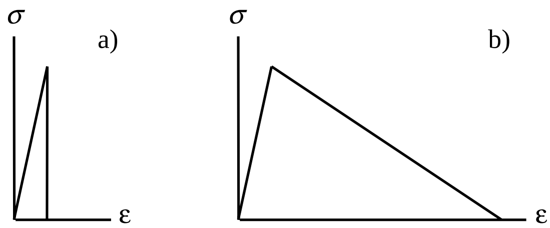

Figure 2 Crack development: a) maximum stress criterion; b) linear softening

failure of FRP structures. As shown in Figure 2, stresses in this approach gradually decrease with increasing strain after reaching a specified value.

The aim of this paper is to describe the models in the Failure Prediction Tool (FPT). Rather than focus on an extensive elaboration of mathematical and computational detail, the main features of the model will be highlighted. The description of the models will proceed by first examining the performance of the softening stress-strain relationship using a fictional test sample. Next, the characteristics of the three failure models are outlined. This is followed by two applications and conclusions.

SOFTENING STRESS STRAIN CURVES

The reason for assuming softening behavior becomes clear when considering the test sample shown in Figure 3. Part of an angle laminate and the bulkhead of a T-joint panel are modeled. A force is applied at the angle. This fictional sample has been analyzed using three finite element meshes. The angle and the bulkhead are connected by interface elements that may fail. Two models for failure are considered: the maximum stress criterion of Figure 2-a and the linear softening behavior of Figure 2-b. Identical material parameters are assumed for each of the three meshes.
When using a maximum stress criterion the material is either elastic or completely failed. The simulated stress distribution along the interface has a discontinuity at the crack tip. At one side stresses are zero and at the other side there is a stress intensity with infinite value at the tip. It is well known that calculated stresses in such a region depend strongly on the element size. For smaller elements the integration points are closer to the crack tip and the stress level is higher. This explains the inconsistency in fracture energy and the mesh dependency observed in Figures 4-a and 5-a. The softening stress strain curves provide a continuous stress distribution along the interface. Elements in front of the crack tip are on the softening branch and stresses gradually increase from zero at the tip to the maximum value in the elastic zone. The continuous stress distribution can be described by the finite element method and results converge upon mesh refinement as shown in Figures 4-b and 5-b.

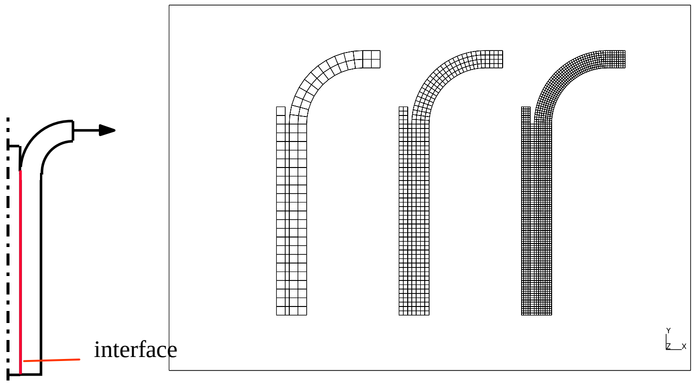

Figure 3 Fictional test sample and finite element meshes (laminates separated to display interface elements)

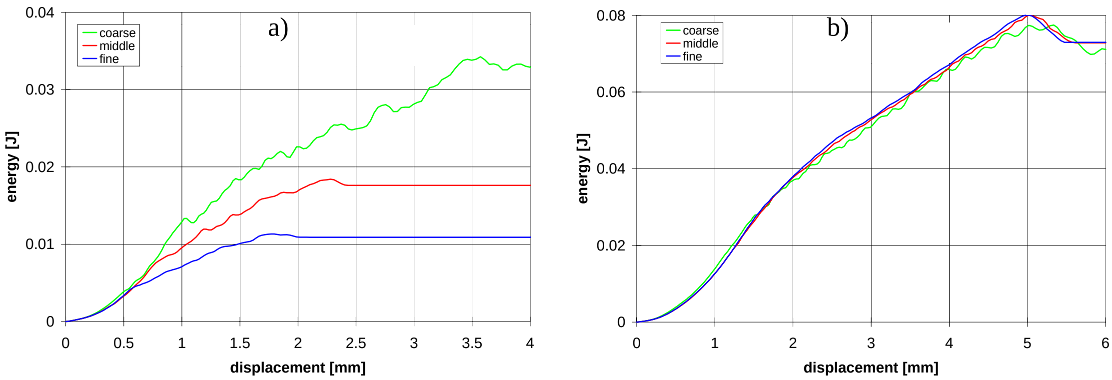

Figure 4 Energy histories: a) maximum stress criterion; b) softening behavior

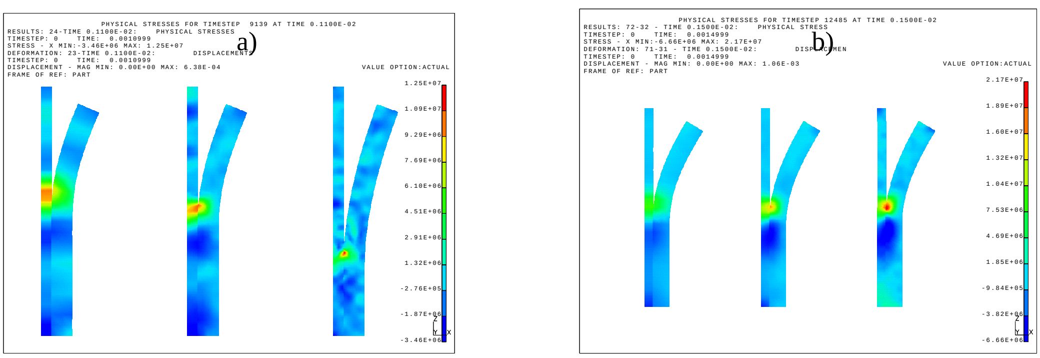

Figure 5 Contours of interlaminar normal stresses plotted on deformed geometry at a given point in time: a) maximum stress criterion; b) softening behavior

DEBONDING FAILURE

Interfaces are weak links in joints and connections. Their strength may be lower due to a higher void content and, more importantly, they usually end in a region containing a stress concentration. The location of bondlines is known beforehand. Therefore a discrete crack model can be applied. The FPT debonding model consists of interface elements and an appropriate constitutive relationship.

A variety of interface elements is available from literature [3]. In the current study a penalty formulation is used that places springs in normal and shear directions. The brittle behavior observed in structural and material tests is

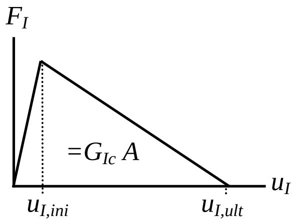

Figure 6 Softening behavior for mode I crack opening (A = crack area represented by the element)

described using the linear softening model shown in Figure 6. The area underneath the traction-displacement curve is related to the critical energy release rate and the area A of the interface element.
In the material response three states can be identified: the elastic or uncracked state; the crack development state and the crack open state. In the initial uncracked state the interface forces are computed from relative displacements assuming linear elastic behavior

$$\mathbf{t} = \begin{Bmatrix} t_I \\ t_{II} \end{Bmatrix} = \begin{bmatrix} k_I & 0 \\ 0 & k_{II} \end{bmatrix} \begin{Bmatrix} u_I \\ u_{II} \end{Bmatrix} = \mathbf{Ku} \tag{1}$$

where the subscripts refer to the crack loading mode. In general the height of the interface equals zero and high penalty values must be assigned to the stiffness terms to model the initial continuous geometry.

The initial linear-elastic state exists until the condition for crack initiation is violated. The criterion used here is based on work of Hashin et al. [4]. For matrix dominated failure modes they derived a quadratic criterion in interlaminar normal and shear stresses. The criterion is valid for unidirectional composites. Ship type laminates are mostly made using heavy woven fabrics. Because of the woven texture of this type of reinforcement the allowable shear stress may increase under increasing normal stress. To account for this the Hashin criterion has been is extended with a friction angle ϕ. The equation for crack initiation becomes

$$f = \left(\frac{\max(t_I, 0)}{S_I} \right)^2 + \left(\frac{t_{II}}{S_{II}\left(1 - \sin(\phi)\min(0, t_I)\right)} \right)^2 = 1 \tag{2}$$

with S_I and S_{II} being allowable forces in normal and shear direction. These ultimate forces are obtained by multiplying the interlaminar normal and shear strength with the area of the interface element.

Upon loading beyond the point of crack initiation the material is assumed to degrade. This is described by incorporation of damage variables D_I and D_{II}. These are monotonically increasing scalar quantities bounded by 0 and 1 that express the level of material degradation. Initially undamaged material is characterized by D = 0, the complete loss of integrity by D = 1. The factor (1-D) represents the stress reduction factor. Normally the damage variables are evaluated independently, evolution of D_I depending upon u_I only and evolution of D_{II} depending upon u_{II} only. For mixed mode loading such an approach results in an overestimation of the locally dissipated energy. As a result thereof the strength of the structure may be overestimated. Therefore a fully interactive formulation has been developed that uses a single internal parameter, α.

For positive crack opening displacements the interactive formulation is obtained by rotating the traction displacement curve of Figure 6 around the force axis towards the slip displacement axes. This is shown in Figure 7-a for positive slip displacements. The force in this Figure is an equivalent force f_e according to Eq. (2). During the rotation the displacements $u_{I,ini}$ and $u_{I,ult}$ are mapped onto $u_{II,ini}$ and $u_{II,ult}$. Two intersecting cones appear. The first has its center in the origin of the u_I, u_{II}, f_e space. Its central axis coincides with the f_e axis. The surface represents points of the initial uncracked state. It is bounded by the second cone which is inclined with the f_e axes. Both will generally be elliptic cones. In the projected view on the u_I, u_{II} plane the crack development state is bounded by two ellipses

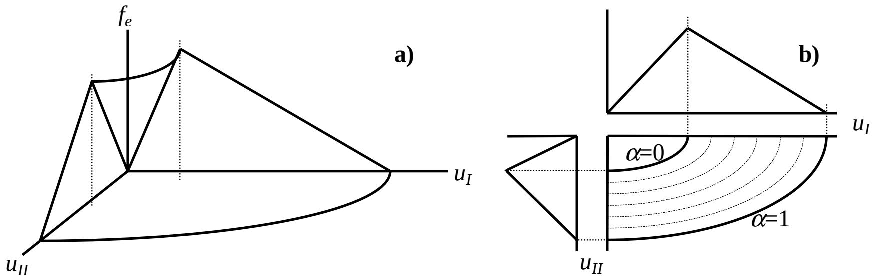

Figure 7 3-D representation of softening model and projected views

representing the initial uncracked state and the completely failed state, see Figure 7-b. In between iso-lines with a constant value of the scalar parameter α may be drawn.
For compressive normal displacements the concept of the friction angle is extended during the damage growth process. The resulting iso-lines for α in the u_I, u_{II} plane are displayed in Figure 8.

The scalar α can be expressed in terms of known displacements u_I and u_{II}. This is a nonlinear equation that has to be solved using an iterative solution procedure. Once α has been obtained interface forces can be computed using the following expression

$$\begin{Bmatrix} t_I \\ t_{II} \end{Bmatrix} = \begin{bmatrix} 1 - D_I(\alpha) & 0 \\ 0 & 1 - D_{II}(\alpha) \end{bmatrix} \begin{bmatrix} k_I & 0 \\ 0 & k_{II} \end{bmatrix} \begin{Bmatrix} u_I \\ u_{II} \end{Bmatrix} \tag{3}$$

with

$$D_I(\alpha) = \frac{\alpha u_{I,ult}}{(1-\alpha)u_{I,ini} + \alpha u_{I,ult}} \quad \text{and} \quad D_{II}(\alpha) = \frac{\alpha u_{II,ult}}{(1-\alpha)u_{II,ini} + \alpha u_{II,ult}} \tag{4}$$

Note that for the undamaged material α equals zero and both D_I and D_{II} are 0. For the completely damaged state α equals 1 and D_I as well as D_{II} are 1.

When an element has completely failed the damage matrix becomes a unit matrix and the resulting stresses from (3) become zero. At this point the crack is considered as open and the element becomes a contact element. Both sides may now separate and come together in an arbitrary way. A contact force is applied to interpenetrating nodes. A rate dependent Coulomb friction is included. The resulting coefficient of friction is given by

$$m = m_k + (m_s - m_k)e^{-\mathrm{b}v_{rel}} \tag{5}$$

where m_s and m_k are the static and the kinetic friction coefficients, b is the transition coefficient governing the rate of change from static friction to kinetic friction, and v_{rel} is the relative velocity between the two surfaces.

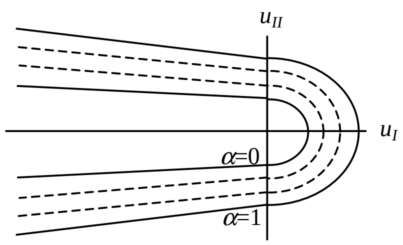

Figure 8 Iso lines of internal parameter α

Tractions in the open crack state follow from

$$\begin{Bmatrix} t_I \\ t_{II} \end{Bmatrix} = \begin{bmatrix} k & 0 \\ m & 0 \end{bmatrix} \begin{Bmatrix} u_I \\ u_{II} \end{Bmatrix} \quad \text{if } u_I < 0 \qquad \text{or} \qquad \begin{Bmatrix} t_I \\ t_{II} \end{Bmatrix} = \begin{Bmatrix} 0 \\ 0 \end{Bmatrix} \quad \text{if } u_I \geq 0 \tag{6}$$

Equations (1), (3) and (6) enable the determination of the interface tractions. The initial stiffness of the interface elements is based on elastic properties of the connected elements. In addition failure stresses and energy release rates need to be specified.

CRACKING OF FILLETS AND INSERTS

The second failure mode is cracking of fillets. Structural fillets are usually made of polymeric resins [5]. For design analysis they can be regarded as isotropic. At lower loading rates the materials exhibit visco-elastic and pressure dependent visco-plastic behavior. In dog bone specimens failure strains of up to 100% are reached. In structures the material is applied in confined situations and the failure strain may be much lower. At the higher loading rates during a shock or blast event, the behavior becomes brittle. Indeed, microscopic investigations of panels tested in the DYCOSS program revealed no permanent set at the fracture surfaces, indicating relatively brittle failure of the fillet material. Defining a failure model that covers the pressure dependent rubbery state and the brittle glassy state was thought to be too ambitious. In deriving and applying such a model one may get lost in defining a mathematically consistent formulation. Also, because of the large number of variables involved, one may lose track of relevant phenomena. Based on the results of microscopic investigations it was decided to assume linear elastic behavior with softening after reaching a damage threshold.

The crack path through a fillet is not known beforehand and has to be predicted by the finite element model. Therefore, the failure model consists of solid elements in conjunction with the softening stress strain curves. The solids available in DYNA3D are eight noded hexahedrons with reduced integration [2]. Elements may be collapsed to obtain wedge or pyramid shapes.

For cracking in solid elements two approaches may be followed. The first is the fixed crack concept. Here the direction of cracking is related to the first occurrence of a principal tensile stress equal to the cracking stress. In subsequent times new principal stresses may arise at some oblique angle that also exceed the crack stress. This may be solved by allowing a set of cracks to occur in each integration point. The resulting models are very complex and difficulties are encountered with the threshold angle at which new cracks may appear [6]. An alternative is the rotating or swinging crack concept introduced by Cope et al. [7]. Here crack directions are related to the current directions of principal strain and therefore rotate in time. This model has an unphysical aspect: cracks cannot rotate. This objection is reduced if one thinks of the rotating crack direction as representing the current most active crack in an area covered by the element, knowing that the stress state in that area is represented by a single Gauss point [8].
In view of the difficulties related to the fixed crack concept, the rotating crack concept has been chosen here.

Despite the fact that detailed meshes are used in the analysis, element sizes are still large compared to crack zones. Figure 9 shows the division in the fillet plotted on one of the failed panels. The damaged zone around a crack falls within the height of a single element and the effect of cracking has to be distributed or 'smeared' over the element. For that reason the model is indicated as the smeared crack model.
Because of this, the degree of tensile softening not only depends on the critical energy release rate, but also on the geometry of elements. More specifically it is related to the 'height' perpendicular to the crack, which is defined as the ratio of the element volume over the area of the crack surface through the element. When doing so an energy consistent

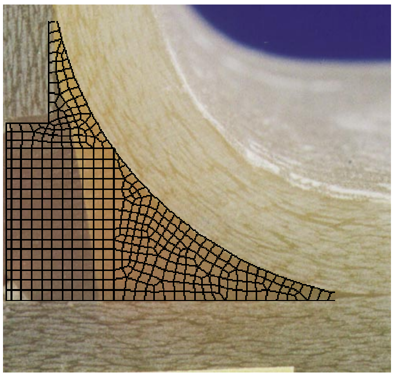

Figure 9 Failed fillet and element mesh

formulation is obtained that provides results that are independent of the element size. This of course is true within certain limits. The slope of the softening branch increases with increasing height. If element dimensions are too large, the maximum stress criterion will be recovered and results become mesh dependent again (the elements have to be converged in the classic elastic sense).

In the above, the basic concepts of the approach have been set. Stresses now have to be determined for given values of strain. For the solution of the element stresses, the concept of equivalent uniaxial strains is applied [9]. It is assumed that damage growth acts on the Young's modulus. The Poisson's ratio is unaffected.

Principal stresses are related to principal strains by

$$\begin{pmatrix}\sigma_1\\ \sigma_2\\ \sigma_3\end{pmatrix}=\frac{E}{(1+\nu)(1-2\nu)}\begin{bmatrix}(1-\nu) & \nu & \nu\\ \nu & (1-\nu) & \nu\\ \nu & \nu & (1-\nu)\end{bmatrix}\begin{pmatrix}\varepsilon_1\\ \varepsilon_2\\ \varepsilon_3\end{pmatrix} \tag{7}$$

which can be expressed as

$$\begin{pmatrix}\sigma_1\\ \sigma_2\\ \sigma_3\end{pmatrix}=\begin{bmatrix}E & 0 & 0\\ 0 & E & 0\\ 0 & 0 & E\end{bmatrix}\begin{bmatrix}d & c & c\\ c & d & c\\ c & c & d\end{bmatrix}\begin{pmatrix}\varepsilon_1\\ \varepsilon_2\\ \varepsilon_3\end{pmatrix}=E\begin{pmatrix}\tilde{\varepsilon}_1\\ \tilde{\varepsilon}_2\\ \tilde{\varepsilon}_3\end{pmatrix} \tag{8}$$

with

$$d=\frac{1-\nu}{(1+\nu)(1-2\nu)} \qquad \text{and} \qquad c=\frac{\nu}{(1+\nu)(1-2\nu)} \tag{9}$$

and $\tilde{\varepsilon}_1,\tilde{\varepsilon}_2,\tilde{\varepsilon}_3$ equivalent uniaxial strains.

In agreement with this linear relationship the nonlinear constitutive behavior is expresses as

$$\begin{pmatrix}\sigma_1\\ \sigma_2\\ \sigma_3\end{pmatrix}=\begin{bmatrix}\overline{E}_1 & 0 & 0\\ 0 & \overline{E}_2 & 0\\ 0 & 0 & \overline{E}_3\end{bmatrix}\begin{pmatrix}\tilde{\varepsilon}_1\\ \tilde{\varepsilon}_2\\ \tilde{\varepsilon}_3\end{pmatrix}=\begin{pmatrix}\overline{E}_1\,\tilde{\varepsilon}_1\\ \overline{E}_2\,\tilde{\varepsilon}_2\\ \overline{E}_3\,\tilde{\varepsilon}_3\end{pmatrix} \tag{10}$$

with $\overline{E}_1,\overline{E}_2$ and $\overline{E}_3$ secant stiffness terms that depend on internal variables.

In the model developed for DYCOSS it has been assumed that there is no interaction between the three directions, in which case stresses simply follow from

$$\sigma_j(\tilde{\varepsilon}_j)=\begin{cases}E\tilde{\varepsilon}_j & \text{if} \quad 0\le\tilde{\varepsilon}_j\le\tilde{\varepsilon}_{j,ini}\\ \sigma_j^t\left(1-\dfrac{\tilde{\varepsilon}_j-\tilde{\varepsilon}_{j,ini}}{\tilde{\varepsilon}_{j,ult}-\tilde{\varepsilon}_{j,ini}}\right) & \text{if} \quad \tilde{\varepsilon}_{j,ini}<\tilde{\varepsilon}_j\le\tilde{\varepsilon}_{j,ult}\\ 0 & \text{if} \quad \tilde{\varepsilon}_j>\tilde{\varepsilon}_{j,ult}\end{cases} \tag{12}$$

with σ_j^t the ultimate stress, $\tilde{\varepsilon}_{j,ini}$ the damage threshold, and $\tilde{\varepsilon}_{j,ult}$ the ultimate strain in *j*-direction (see also Figure 2).

As long as the element is not completely failed, deformations are relatively small. For this situation crack closure is included, meaning that the initial stiffness is recovered for compressive loading. Once the element has completely failed large distortions may occur. Considering crack closure for these situations may introduce instabilities and is therefore omitted for the open crack state.

DELAMINATION FAILURE

Features for the delamination model are basically obtained by combining items mentioned in the previous sections. As for cracking of fillets, it is not known beforehand at which location the damage will occur. This has to be predicted by the finite element model and a method that uses solid elements is required. Defect directions, however, are now channeled by the plies. Stresses may be evaluated with respect to the coordinate system defined by the principal material directions. Failure of the laminates is brittle and linear softening behavior may be assumed. A model has been defined in which damage evolution is based on interlaminar normal and shear strains. Contributions of in-plane deformations are not included because simulations indicate that in-plane strains are small compared to ultimate values obtained from material tests. As for the discrete crack model, a friction angle is included for compressive normal stresses. For reasons mentioned earlier, crack closure is only considered when the element is not completely failed.
Stresses are evaluated using a return mapping procedure defined in [10]. The approach basically consists of defining one or more failure surfaces. Based on the total strains a first elastic trial stress is computed. If the stress state is outside one of the failure surfaces a return step is performed introducing inelastic strains.

APPLICATIONS

In a related paper on the DYCOSS program, simulations of shock table tests are presented [1]. In that paper calculated displacements and strains are compared with measured data and the simulated damage is compared with the observed pattern. Two more cases follow below. This first is not really an application but more a comparison between results obtained using different methods for progressive failure. In the second example failure in a panel with a foam insert is considered.

Quasi static loading of T-joint panel
Figure 10 shows a T-joint panel loaded at the bulkhead by a prescribed displacement. The base panel is simply supported at its ends. This quasi-static problem has been analyzed using maximum stress criteria and the models in the FPT. Two meshes with different element sizes have been considered. Although not realistic for an actual panel, symmetry conditions were used in these simulations as it concerns a comparison between different methods. For the stress criteria, only the ultimate stresses are required. Identical data are used in both meshes.

Figure 11 and 12 give results. Deformed configurations for both meshes are plotted for a series of bulkhead displacements. Failed elements have been removed. The performance of the softening models is evident, providing nearly identical results for both meshes. The maximum stress criterion clearly suffers from mesh dependency. Also, in these simulations stability problems were encountered.
Note that the displacement at complete failure of elements is considerably larger for the softening models. The ultimate strain for these models is much higher, as shown in Figure 2. In both simulations damage initiation (=reaching ultimate stress) will occur at the same displacement.

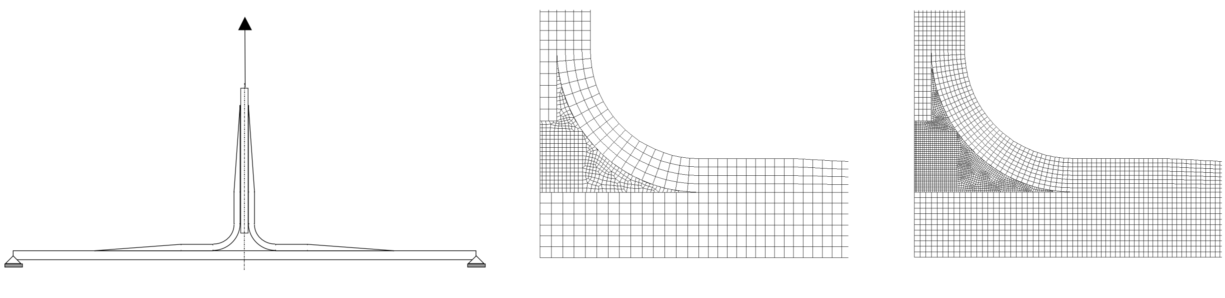

Figure 10 T-joint panel loaded at bulkhead a details of finite element meshes

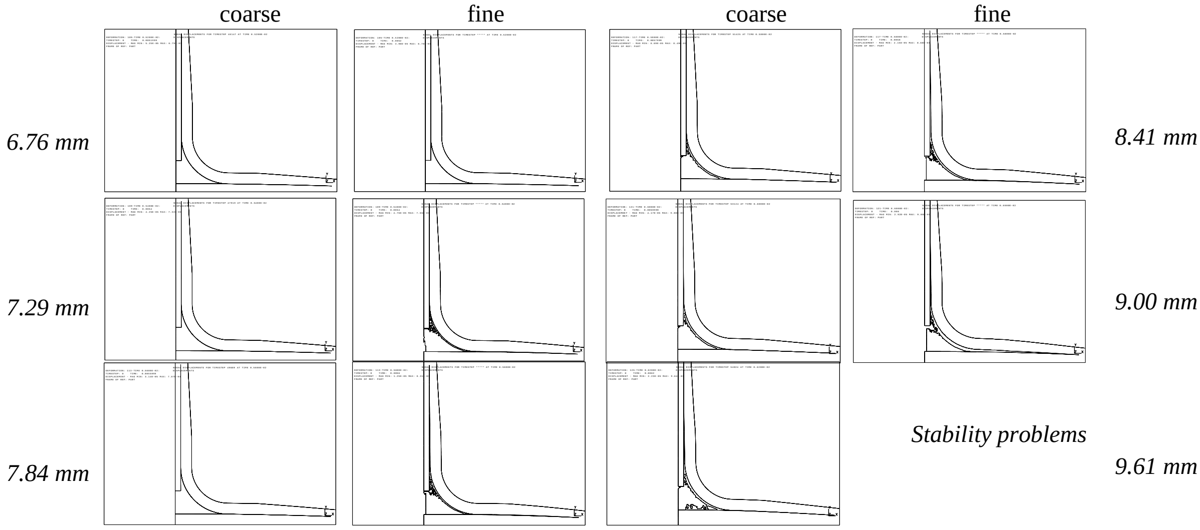

Figure 11 Deformed configurations obtained with maximum stress criterion (failed elements removed)

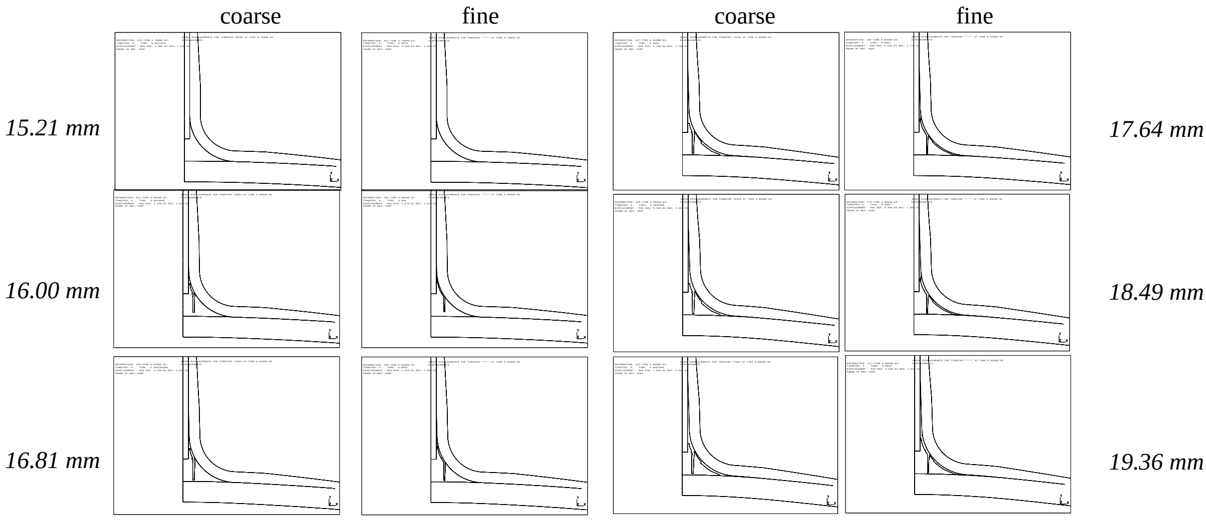

Figure 12 Deformed configurations obtained with models in FPT (failed elements removed)

Failure of joint with foam insert

One of the panel configurations tested in DYCOSS is a T-joint panel with a foam insert in the joint. This design must be regarded as an alternative to more conventional T-joint designs with a smaller radius. In addition, the edge of the bulkhead has been trimmed. One of the shock table tests for this panel has been analyzed using the FPT. The finite element model is shown in Figure 13. The foam material is simulated using the model for cracking of fillets. The calculated damage progression is depicted in Figure 14. Damage initiates in tip of the fillet (polymeric material) between the angle laminate and the foam insert. Cracking starts in a later phase of the response when the mass on the bulkhead is decelerated and the joint is loaded in tension. The tensile load on the joint tends to straighten the angle laminate. Due to differences in stiffness between the foam material and the polymeric material large strains occur in the fillet tip. After initiation, the crack runs upward. This is because the critical energy release rate of the fillet material is low compared to the value of the linearized PVC foam. Later the crack also propagates through the foam. Comparison with the observed damage shows good agreement.

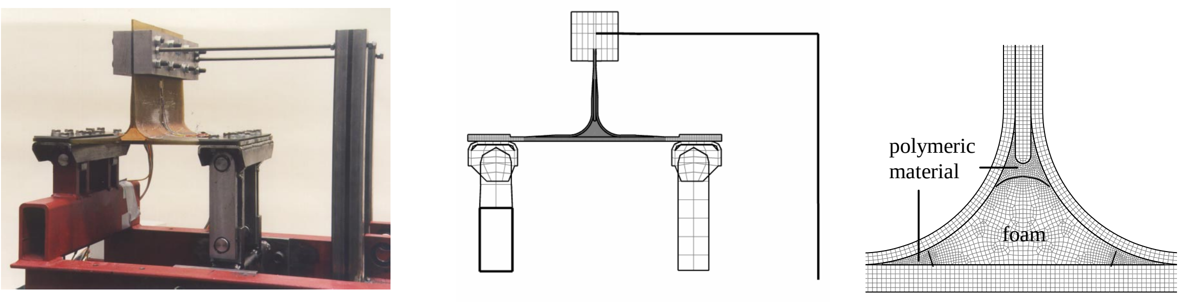

Figure 13 Test arrangement and finite element model of TR-joint with foam insert

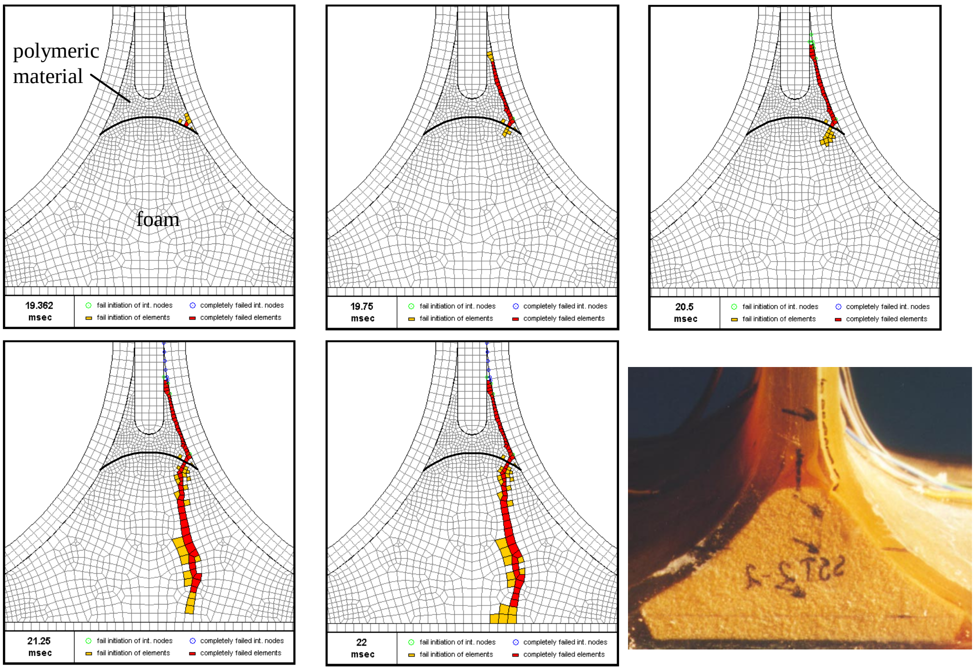

Figure 14 Calculated damage progression and photograph of failed panel

CONCLUSIONS

Methods have been presented for modeling brittle failure in ship structures of fibre composite materials. Three failure modes have been considered: debonding failure along material interfaces, cracking of fillets, and delamination in the composite material itself. Separate models have been defined for each of these modes. For the debonding failure, a discrete crack model has been defined that can describe progressive failure under mixed mode loading. This method employs interface elements in conjunction with a softening relationship between interface forces and interface displacements. For failure of isotropic fillets and inserts, a smeared crack concept is applied which uses solid elements and softening stress-strain relationships. Stresses are evaluated in principal strain directions. For delamination of the composite material itself, a nearly identical formulation is applied. Since defects will be channeled by the plies, stresses for this model are evaluated in principal material directions. In each of the models fracture mechanics is introduced by relating the areas under the stress-strain curve to the critical energy release rates. The models require material strengths and these critical energy release rates as input.

The performance of the models has been illustrated by two examples. Comparison between results for different element sizes shows that the models provide mesh independent results. Comparison with experimental observations shows that the models are capable of predicting realistic damage patterns, even for complicated failure mechanisms.

ACKNOWLEDGEMENTS

This work has been supported by the Office of Naval Research, the Netherlands Ministry of Defense and TNO. The authors would like to thank Mr. J. Gagorik and Dr. Roshdy Barsoum of ONR, Dr. J. Corrado, Dr. D. Palmer and Dr. M.O. Critchfield of NSWCCD, and Mr. P.J. Keuning and Mr. T.N. Bosman of the Royal Netherlands Navy for their help in performing this project. Special thanks to Dr. P. H. Feenstra of TNO for the instructive and fruitful discussions on the failure models.

REFERENCES

[1] Meijer, G.J., Rasmussen, E.A., Lemmen, P.P.M., Lemmen, R.L.C., and Palmer, D., "Dynamic Behavior of Composite Ship Structures (DYCOSS) Test and Analysis Effort", *70th Shock and Vibration Symposium*, New Mexico 1999.

[2] Whirley, R.G. and Hallquist, J.O., *DYNA3D A Non-Linear, Explicit, Three-Dimensional Finite Element Code for Solid and Structural Mechanics – User Manual*, Lawrence Livermore National Laboratory, UCRL-MA-107254, May 1991.

[3] Schellekens, J.C.J., and de Borst, R., 1993, "On the Numerical Integration of Interface Elements", Int. Journal for Numerical Methods in Engineering, Vol. 36, pp. 43-66.

[4] Hashin, Z. 1980, "Failure criteria for unidirectional fiber composites", *Journal of Applied Mechanics*, Vol. 47, pp. 329-334

[5] Shenoi, R.A., and Hawkins, G.L., 1992, "Influence of Material and Geometry Variations on the Behavior of Bonded Tee Connections", *Composites*, Vol. 23, pp. 335-345.

[6] de Borst, R., and Nauta, P., 1985, "Non-orthogonal cracks in a smeared finite element model", *Engineering Computations*, Vol. 2, pp. 35-46.

[7] Cope, R.J., Rao, P.V., Clark, L.A., and Norris, P., 1980, *Modelling of reinforced concrete behaviour for finite element analysis of slabs*, ed. C. Taylor et al., Pineridge Press, Swansea, Vol. 1, pp. 457-470.

[8] Crisfield, M. A., 1998, *Nonlinear finite element analysis of solids and structures volume 2 advanced topics*, John Wiley & Sons.

[9] Feenstra, P.H., Rots, J.G., Arnesen, A., Teigen, J.G., and Hoiseth, K.V., 1998, "A 3-d constitutive model for concrete based on a co-rotational concept", *Computational modelling of concrete structures, proceedings of the euro-c 1998 conference*, ed. R. de Borst, N. Bicanic, H. Mang, and G. Meschke, AA Balkema Rotterdam.

[10] Feenstra, P.B., 1993, *Computational Aspects of Biaxial Stress in Plain and Reinforced Concrete*, Ph.D. thesis, Delft University of Technology, Delft.